nature communications

Article

https://doi.org/10.1038/s41467-026-76233-9

Nutrient starvation and phosphonate utilization coordinate buoyancy and high-light tolerance in *Trichodesmium*

Received: 3 March 2026

Accepted: 10 July 2026

Published online: 05 August 2026

Check for updates

Chuze Zou (邹楚泽)[1], Guang Gao (高光)[1], Xin Lin (林昕)[1], Mina Bizic[2], Ilana Berman-Frank[3] & Kunshan Gao (高坤山)[1,4]

The formation of surface blooms by the diazotrophic cyanobacterium *Trichodesmium* contributes extensively to carbon and nitrogen cycling. Yet the physiological drivers governing its vertical ascent and subsequent tolerance to high surface irradiance remain obscure. By measuring sinking and floating velocities, analyzing transcriptome responses, and tracking the subcellular distribution of gas vesicles, we show that nutrient starvation is the primary trigger for vertical ascent. Specifically, iron or phosphorus depletion inhibits metabolic ballasting, disrupting the equilibrium with gas vesicle lift and driving *Trichodesmium* towards surface waters. Moreover, this vertical migration is safeguarded by a light-dependent metabolic "safety brake" that prevents irreversible sinking to the deep ocean. Upon reaching the surface, *Trichodesmium* shifts to utilizing alternative organic phosphorus sources. Particularly, the utilization of methylphosphonate (MPn) activates a distinct "surface-survival mode" characterized by the downregulation of photosynthetic activity and the relocalization of gas vesicles to form peripheral optical shields. Our findings reveal a coordinated strategy linking nutrient sensing, buoyancy regulation, and photoprotection, explaining how *Trichodesmium* secures its ecological success under the high irradiance of the oligotrophic surface oceans.

T richodesmium is a globally significant diazotroph, contributing up to half of the total biological nitrogen fixation in oligotrophic subtropical and tropical oceans[1,2]. It forms extensive surface blooms that release bioavailable nitrogen[3–6], fueling marine microbial food webs and sustaining primary productivity in nitrogen-limited waters[7–9]. A defining characteristic of *Trichodesmium* is its ability to vertically migrate within the euphotic zone, allowing populations to access deep nutrient pools while inhabiting the surface waters[10–12].

For decades, these vertical dynamics have been interpreted through the carbohydrate model[11–14]. In this paradigm, gas vesicles confer baseline positive buoyancy[15–17], which is then modulated by the diel accumulation and consumption of carbohydrate ballast[11,18]. While this model explains daily migration cycles, it is contradicted by the persistence of surface blooms, where populations defy the gravity-driven sinking expected from carbohydrate accumulation and remain buoyant.

Extended residence within the surface waters exposes *Trichodesmium* to inhibitory, and often lethal, solar radiation[1,19,20]. To cope, *Trichodesmium* employs a suite of photoprotective strategies: colony formation provides self-shading for internal

[1]State Key Laboratory of Marine Environmental Science, College of the Environment and Ecology, Xiamen University, Xiamen, China. [2]Department of Environmental Microbiomics, Technical University of Berlin, Berlin, Germany. [3]Department of Marine Biology, Leon H. Charney School of Marine Sciences, University of Haifa, Haifa, Israel. [4]Co-Innovation Center of Jiangsu Marine Bio-industry Technology, Jiangsu Ocean University, Lianyungang, China.
e-mail: ksgao@xmu.edu.cn

https://doi.org/10.1038/s41467-026-76233-9

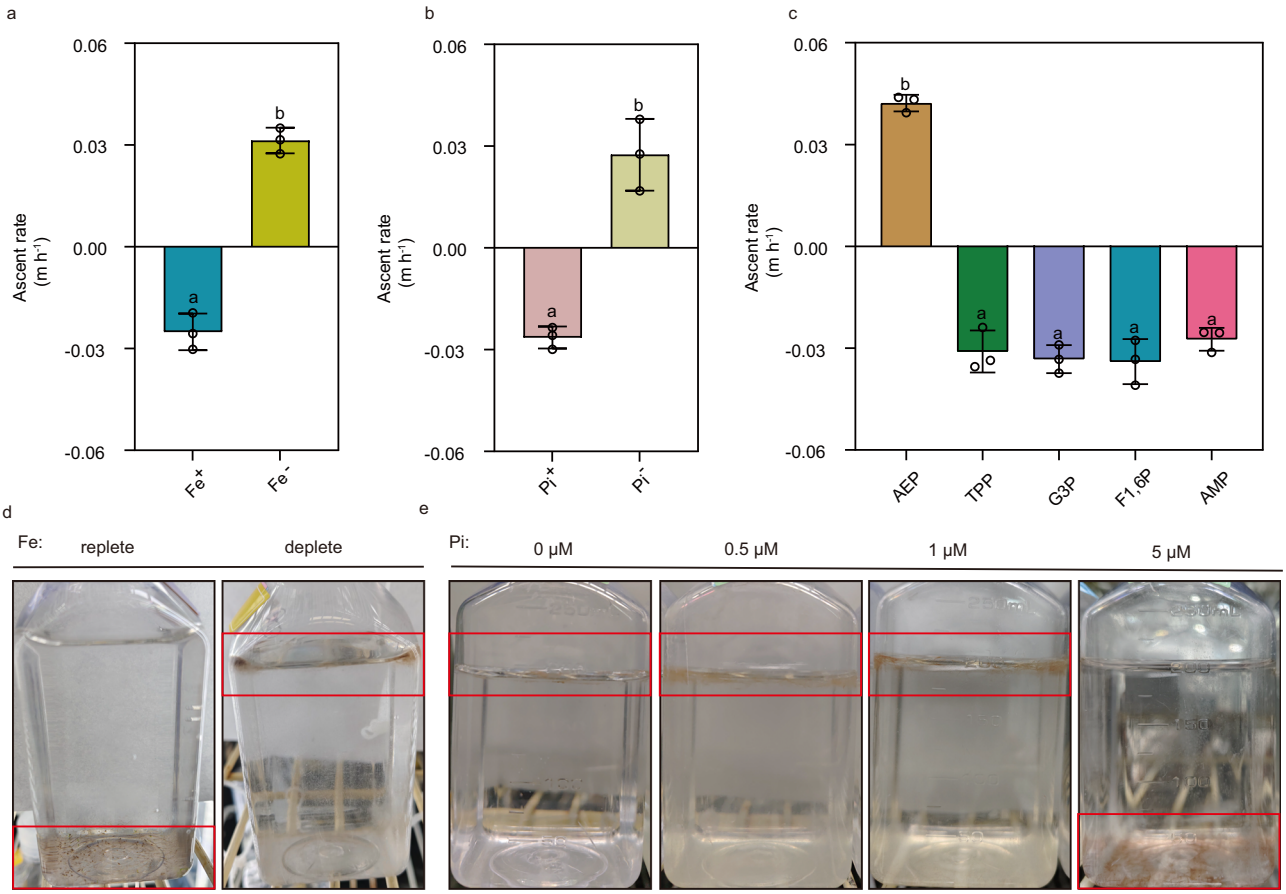


Fig. 1 | Nutrient availability regulates buoyancy in *Trichodesmium* IMS 101. **a**–**c** Vertical ascent rates of *Trichodesmium* grown under different nutrient conditions: iron-replete (Fe^+) versus iron-deplete (Fe^-, **a**); phosphate-replete (Pi^+) versus phosphate-deplete (Pi^-, **b**); and varying organic phosphorus sources **c**. Data are mean ± sd ($n = 3$ biologically independent samples). Different letters denote statistically significant differences (for a,b two-sided unpaired Student's t-test, $p = 0.0001$, $p = 0.001$; for c, one-way ANOVA followed by two-sided Tukey's post hoc multiple comparison test, AEP differs significantly from TPP, G3P, F1,6 P, and AMP, all $p < 0.0001$). **d**, **e** Vertical distribution of *Trichodesmium* after two weeks of batch culture. **d** Comparison between iron-replete (bottom) and iron-deplete (surface) conditions. **e** Response to a gradient of phosphate concentrations (0–5 µM). Red frames highlight the primary depth distribution of biomass. Fe, iron; Pi, phosphate; AEP, aminoethylphosphonate; TPP, tripolyphosphate; G3P, glycerol 3-phosphate; F1,6P, fructose-1,6-bisphosphate; AMP, adenosine monophosphate. Source data are provided as a Source Data file.

trichomes[21], while gas vesicles in *Trichodesmium erythraeum* IMS101 are peripherally arranged, acting as optical barriers to scatter excessive incident light[17,22]. These structural barriers are further bolstered by robust physiological defenses, including antioxidant systems and thermal dissipation[23–25]. Yet, a critical gap remains. It is unknown how *Trichodesmium* coordinates these high-light adaptations with buoyancy regulation to override metabolic ballasting, thereby allowing it to persist under high intensities of incident sunlight in tropical surface oceans.

Trichodesmium sometimes loses buoyancy regulation and is sensitive to high light under laboratory conditions[24,26]. This phenotypic shift led us to hypothesize that specific environmental factors govern these traits. Here, we demonstrate that nutrient status (specifically Fe and P depletion) and light intensity jointly regulate buoyancy in *T. erythraeum* IMS101 by modulating the equilibrium between cellular ballasting and gas vesicle lift. Moreover, we identify that methylphosphonate (MPn), a specific component of the dissolved organic phosphorus pool in oligotrophic surface waters[27–29], initiates a physiological response that promotes surface retention and confers resilience to high light. These findings provide a mechanistic explanation for buoyancy regulation and survival under intense surface irradiance.

Results

Interactive regulation of buoyancy by nutrient status and light intensity

Nutrient starvation drives surface retention. To determine the primary regulators of vertical migration, we examined the impact of nutrient status, specifically iron (Fe) and phosphorus (P) availability. In Fe-replete cultures, filaments exhibited a net sinking phenotype (descent rate: 0.025 ± 0.005 m h^{-1}; Figs. 1a, 1d). Conversely, Fe depletion triggered a buoyancy reversal, resulting in an ascent rate of 0.031 ± 0.004 m h^{-1}. We observed a similar response under P limitation (Figs. 1b, 1e); filaments descended under phosphate-replete conditions (5 µM), whereas P depletion consistently triggered ascent. The timing of this ascent varied with initial phosphorus concentration (0-1 µM). This was confirmed in semi-continuous cultures, where limiting phosphate (0.5 µM) drove ascent rates of 0.021 ± 0.011 m h^{-1}. P-limited conditions resulted in significantly reduced cellular C, N, and P assimilation (Supplementary Figs. 1a-c; $p < 0.0001$, $p = 0.0007$, $p = 0.0007$, respectively), indicating that metabolic restriction limits the accumulation of cellular ballast, thereby tipping the balance toward gas vesicle-mediated buoyancy.

Phosphonates trigger positive buoyancy. Considering the diversity of dissolved phosphorus forms in the ocean beyond the commonly studied inorganic phosphate, we investigated the specific effects of

https://doi.org/10.1038/s41467-026-76233-9

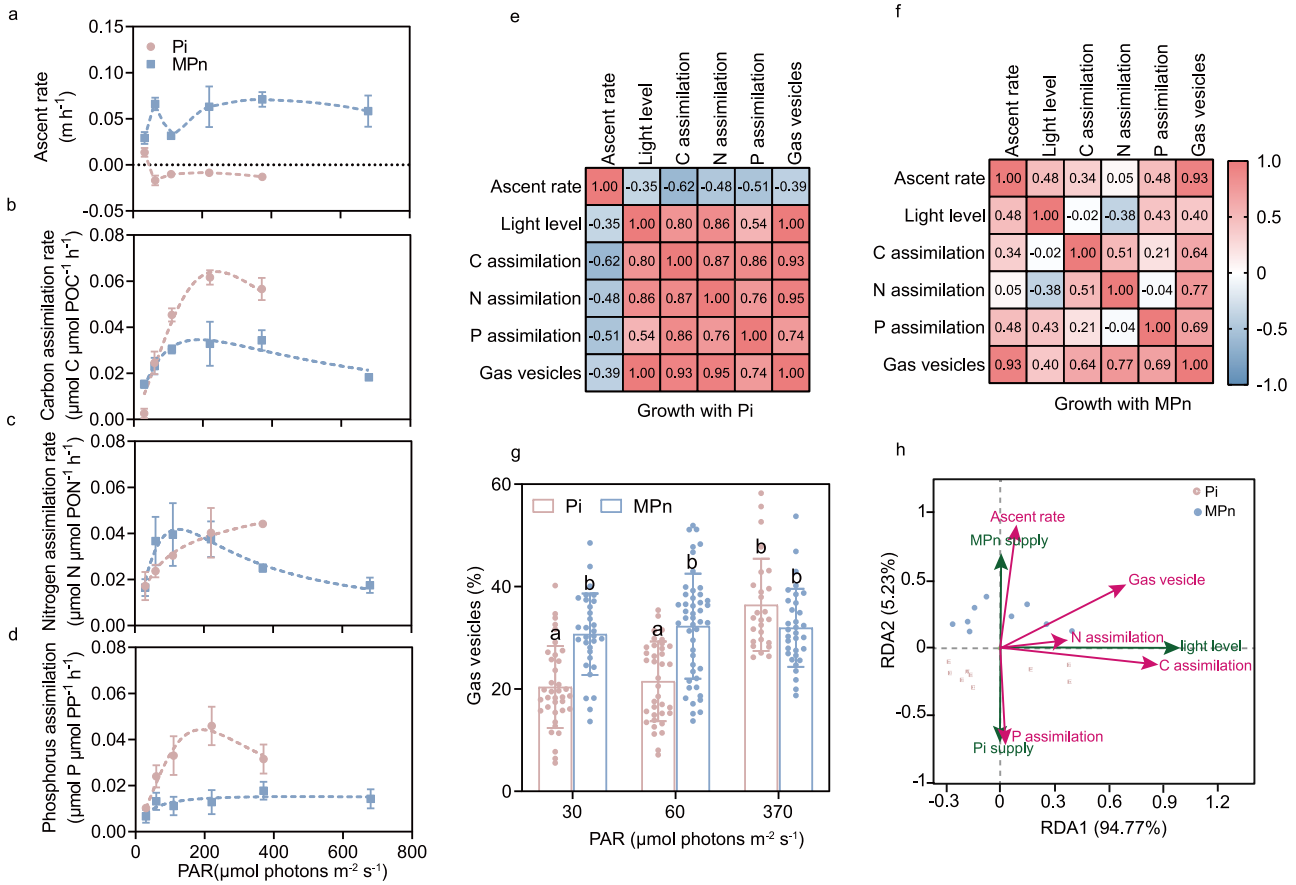


Fig. 2 | Interactive effects of light intensity and phosphorus source on *Trichodesmium* buoyancy and metabolism. a–d Physiological responses to light intensity. Vertical ascent rates (**a**) and assimilation rates of carbon **b**, nitrogen **c**, and phosphorus **d** measured during the light period. Data in a-d are presented as mean ± sd ($n = 3$ biologically independent samples). **e**, **f** Heatmaps of Pearson correlation coefficients between physiological parameters in Pi-grown **e** and MPn-grown **f** cultures. Red indicates positive correlation; blue indicates negative correlation. **g** Relative gas vesicle volume fraction quantified from transmission electron microscope images. Data are presented as mean ± sd (analyzed cell numbers: $n = 37, 37, 26$ Pi-grown cultures, and $n = 31, 47, 33$ for MPn-grown cultures at 30, 60, and 370 μmol photons m^{-2} s^{-1} μmol photons m^{-2} s^{-1}, respectively). Different letters denote statistically significant differences between Pi- and MPn-grown cultures (two-way ANOVA followed by two-sided Tukey's post hoc multiple comparison test). **h** Redundancy analysis (RDA) biplot showing the relationship between environmental factors (green arrows: MPn/Pi supply, light level) and physiological variables (magenta arrows). Source data are provided as a Source Data file.

different forms of P on buoyancy. Several labile P sources, including tripolyphosphate (TPP) and organic phosphoesters (glycerol-3-phosphate, fructose-1,6-bisphosphate, and adenosine monophosphate), consistently sustained high assimilation rates and a sinking phenotype (Fig. 1c, Supplementary Figs. 1d-f). In contrast, phosphonates—specifically methylphosphonate (MPn) and aminoethylphosphonate (AEP)—induced positive buoyancy (Figs. 1c and 2a).

Light intensity regulates buoyancy via metabolic ballasting . Under phosphate-replete conditions, *Trichodesmium* exhibited a light-dependent buoyancy response driven by cellular ballast accumulation. Specifically, at light intensities from 60 to 370 μmol photons m^{-2} s^{-1}, filaments sank with descent rates ranging from 0.009 to 0.017 m h^{-1} (Fig. 2a). These rates were negatively correlated with carbon and phosphorus assimilation but independent of gas vesicle content (Fig. 2a–e; carbon: $r = -0.62$, $p = 0.014$, phosphorus: $r = -0.51$, $p = 0.049$, gas vesicle: $r = 0.39$, $p = 0.293$, respectively). Under low light (30 μmol photons m^{-2} s^{-1}), this regime reversed, with filaments ascending at 0.014 ± 0.005 m h^{-1} (Fig. 2a). The ascent was coupled with a significant reduction in C and P assimilation compared to filaments cultured at 60 μmol photons m^{-2} s^{-1} (Fig. 2b, d; $p < 0.0001$, $p = 0.049$), while gas vesicle content remained constant (Fig. 2g; $p = 0.999$). We define this transition threshold, occurring at >30 μmol photons m^{-2} s^{-1} (approximating a depth of <80 m)[30], as the buoyancy compensation depth (BCD).

MPn shifts buoyancy control from ballast to gasvesicle . Under MPn enrichment, *Trichodesmium* maintained consistently positive buoyancy across all growth acclimated light intensities (ascent rates: 0.029–0.071 m h^{-1}; Fig. 2a), which was accompanied by significantly lower carbon and phosphorus assimilation compared to Pi-grown filaments (Fig. 2b, d; $p < 0.0001$, $p < 0.0001$). These cultures also retained elevated gas vesicle content even under low light (Fig. 2g; $p < 0.0001$). Consequently, ascent rates became positively correlated with gas vesicle content rather than carbon and phosphorus assimilation (Fig. 2f; gas vesicle: $r = 0.93$, $p < 0.0001$, carbon: $r = 0.34$, $p = 0.168$, phosphorus: $r = 0.48$, $p = 0.054$). Redundancy analysis (RDA) identified gas vesicle content as a positive predictor of buoyancy, while carbon and phosphorus assimilation were negative predictors (Fig. 2h). This confirmed a regime shift where the presence of gas vesicles superseded metabolic ballast as the primary buoyancy driver in MPn-grown cultures. While our observed ascent rate (~ 0.07 m h^{-1}) is lower than the instantaneous velocities reported for large colonies or for *Trichodesmium* undergoing programmed cell death (~ 2.5 m h^{-1})[15,19,31], it aligns closely with the net vertical

https://doi.org/10.1038/s41467-026-76233-9

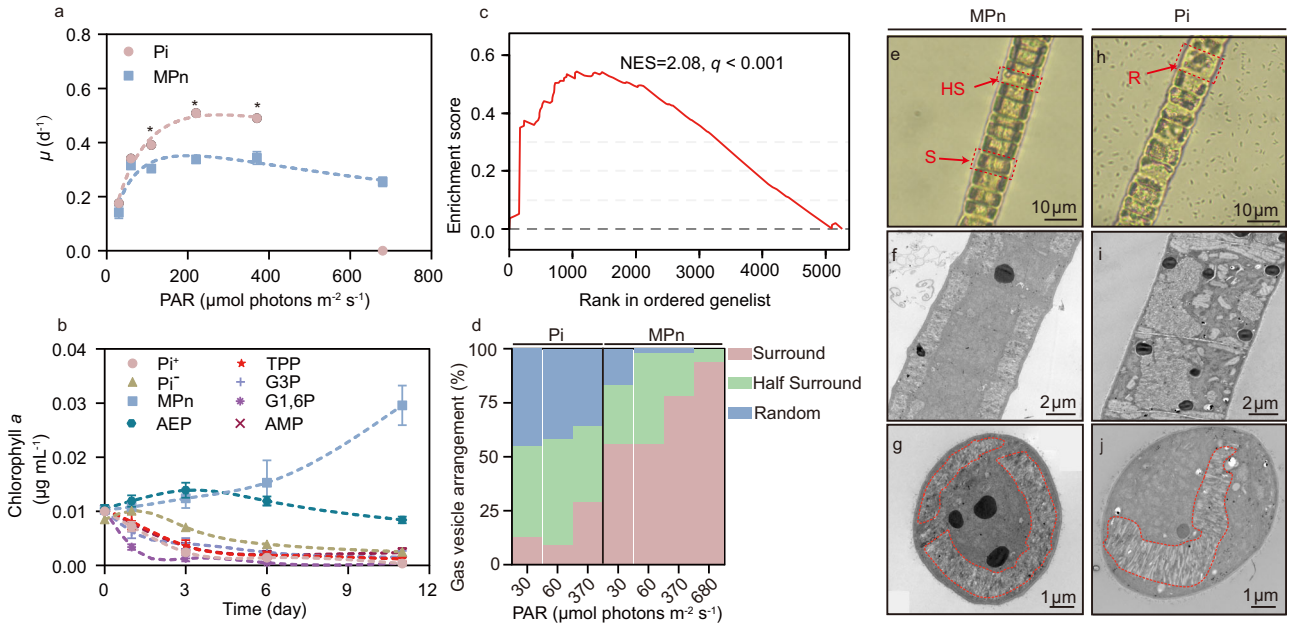


Fig. 3 | Utilization of methylphosphonate enhances high-light tolerance in *Trichodesmium*. **a** Specific growth rates of *Trichodesmium* after 12 months of acclimation to light intensities ranging from 30 to 680 μmol photons m^{-2} s^{-1} (two-way ANOVA followed by Tukey's multiple-comparison test). Asterisks (*) indicate significant differences between Pi- and MPn-grown cultures at 110, 220, and 370 μmol photons m^{-2} s^{-1} (all $p < 0.0001$). **b** High light tolerance assay. *Trichodesmium* cultures were grown for two months with different phosphorus sources before exposure to extreme light (900 μmol photons m^{-2} s^{-1}). Data in **a** and **b** are presented as mean ± sd ($n = 3$ biologically independent samples). **c** Gene set enrichment analysis (GSEA) revealing significant upregulation of a cell differentiation gene set in MPn-grown cultures. NES, normalized enrichment score; *q*, false discovery rate. **d**, Frequency distribution of gas vesicle positioning across different light intensities (analyzed cell numbers: $n = 414$, 379, 371 for Pi-grown cultures, and $n = 460$, 370, 345, 332 for MPn-grown cultures at 30, 60, 370, and 680 μmol photons m^{-2} s^{-1}, respectively). **e**–**j** Gas vesicle arrangement in MPn-grown cells (**e**–**g**)) and phosphate-grown cells (**h**–**j**) at 370 μmol photons m^{-2} s^{-1}. **e**, **h** Optical micrographs (scale bars, 10 μm); **f, i** Transmission electron microscopy (TEM) longitudinal sections (scale bars, 2 μm); **g, j** TEM cross-sections (scale bars, 1 μm). Micrographs are representative of cells pooled from three biologically independent cultures, with similar gas vesicle arrangements observed in multiple fields of view (corresponding quantitative data and sample sizes are shown in Fig. 2g). S, surround (peripheral); HS, half-surround (semi-peripheral); R, random arrangement. Red arrows and dashed outlines indicate the gas vesicles. Pi^+, phosphate replete; Pi^-, phosphate deplete; MPn, methylphosphonate; AEP, aminoethylphosphonate; TPP, tripolyphosphate; G3P, glycerol 3-phosphate; F1,6P, fructose 1,6-bisphosphate; AMP, adenosine monophosphate. Source data are provided as a Source Data file.

migration rates (~0.1 m h^{-1}) derived from field studies[15], which account for the bidirectional nature of vertical movement[11,12].

Mechanisms enabling *Trichodesmium* to survive under high light

MPn utilization confers physiological resilience to high light. In the ocean, *Trichodesmium* experiences a broad range of light intensities, from depths receiving less than 0.1% of surface photosynthetically active radiation (PAR) to tropical surface waters, where midday irradiance can exceed 2000 μmol photons m^{-2} s^{-1}. Here, we show that *Trichodesmium* grown under light intensities of 30–370 μmol photons m^{-2} s^{-1} exhibited slower growth when utilizing MPn (0.14–0.34 d^{-1}) compared to phosphate (0.18–0.51 d^{-1}; Fig. 3a; $p < 0.0001$). However, under a light intensity of 680 μmol photons m^{-2} s^{-1}, phosphate-grown cultures collapsed, whereas MPn-grown cultures sustained a robust growth rate of 0.26 ± 0.02 d^{-1}. This resilience was corroborated by acute high-light exposure assays. Cultures pre-acclimated for 2 months at 150 μmol photons m^{-2} s^{-1} were exposed to 900 μmol photons m^{-2} s^{-1} for 11 days. Under this high-light treatment, those supplied with MPn demonstrated robust growth, while those with aminoethylphosphonate (AEP) maintained stable biomass. Conversely, P-limited cultures and those relying on phosphate, polyphosphates, or phosphate esters, collapsed (Fig. 3b).

MPn utilization induces gas vesicle rearrangement to form a light-protective barrier. To elucidate the underlying mechanisms of these characteristics, we performed transcriptomic analysis. Principal component analysis (PCA) of the transcriptomic profiles revealed distinct gene expression patterns driven by phosphorus source and light intensity (Supplementary Fig. 2). Gene set enrichment analysis (GSEA) showed significant upregulation of a cell differentiation (sporulation-annotated) gene set in MPn-grown cultures (Fig. 3c; NES = 2.08, *q*-value < 0.001), which may reflect intracellular morphogenetic remodeling rather than terminal cellular differentiation (e.g. cysts or spores) that is not typically observed in *Trichodesmium*. Consistent with these transcriptomic changes, microscopy revealed a re-localization of gas vesicles to the cell periphery in MPn-grown cells, forming a perimeter around the central cytoplasm that functions as a light-protective barrier (Fig. 3e-g). This configuration was light-dependent, increasing in frequency from 56% of cells at low light to 94% at high light (Fig. 3d), aligning with observations in natural *T. erythraeum* populations from surface waters[22]. In contrast, gas vesicles in phosphate-grown cells were predominantly randomly distributed (Fig. 3h-j), with only 9–29% of cells exhibiting the peripheral arrangement across all tested light intensities (Fig. 3d), a finding consistent with previous reports[32]. Similarly, this random arrangement persisted even under prolonged P-depleted conditions (after two-months of pre-culture, Supplementary Fig. 3), with only ~12% of cells exhibiting the peripheral configuration.

Coordinated dampening of photosynthesis minimizes oxidative stress under MPn utilization. In addition to the reorganized cellular arrangement of gas vesicles, MPn utilization induced a distinct physiological shift in photosynthetic performance. Compared to

https://doi.org/10.1038/s41467-026-76233-9

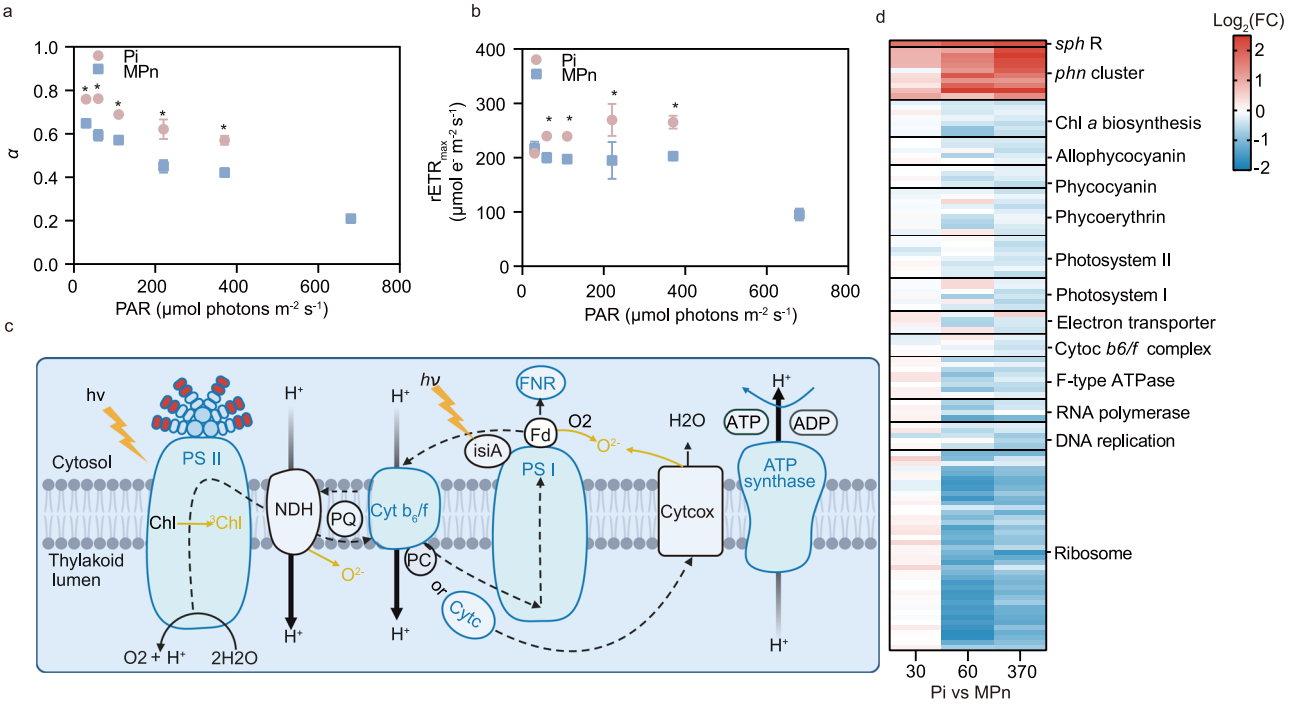


Fig. 4 | Coordinated downregulation of photosynthesis and biosynthetic machinery in MPn-grown *Trichodesmium*. **a, b**, Photosynthetic parameters derived from fluorescence-based photosynthesis irradiance curves (P-I curves): relative photosynthetic light-harvesting efficiency (initial slopes, α; **a**) and maximum relative electron transport rate ($rETR_{max}$; **b**) of *Trichodesmium* grown with phosphate (Pi) or methylphosphonate (MPn). Data are presented as mean ± sd ($n = 3$ biologically independent samples). Asterisk (*) indicates significant differences between Pi- and MPn-grown cultures at individual light intensities (two-way ANOVA followed by Tukey's multiple-comparisons test; for α, $p < 0.0001$ at all light intensities; for $rETR_{max}$, $p = 0.03$, $p = 0.02$, $p < 0.0001$, $p = 0.0006$ at 60, 110, 220, 370 µmol photons m^{-2} s^{-1}, respectively). **c** Schematic illustrating the downregulation of the photosynthetic apparatus in MPn-grown cells compared to Pi-grown cells under light intensity of 370 µmol photons m^{-2} s^{-1}. Protein complexes encoded by downregulated genes are highlighted in blue. Created in BioRender. Zou, C. (2026) https://BioRender.com/3y94q2. **d** Heatmap profiling the differential expression (log_2 fold changes) of genes related to phosphonate metabolism, photosynthesis, DNA replication and protein synthesis in MPn-grown cells compared to Pi-grown cells under light intensities of 30, 60, and 370 µmol photons m^{-2} s^{-1} (after 12 months of acclimation). Red indicates upregulation; blue indicates downregulation. *hv*, light photons; PSII, photosystem II; PSI, photosystem I; Chl *a*, chlorophyll a; NDH, NAD(P)H dehydrogenase; PQ, plastoquinone; Cyt b_6f, cytochrome b_6f complex; PC, plastocyanin; Cyt *c*, Cytochrome *c*; $Cytc_{ox}$, Cytochrome *c* oxidase; Fd, ferredoxin; FNR, ferredoxin-NADP reductase; isiA, photoprotective protein. Source data are provided as a Source Data file.

phosphate-grown cultures, MPn-grown cells exhibited reduced initial slopes of the photosynthesis-irradiance curves (α) and suppressed maximum electron transport rates ($rETR_{max}$) (Fig. 4a, b; $p < 0.0001$, $p < 0.0001$). Transcriptomic analysis confirmed a coordinated global repression of the photosynthetic machinery, characterized by the downregulation of transcripts encoding chlorophyll-*a* biosynthesis enzymes, phycobilisome antenna complexes (phycocyanin, allophycocyanin, and phycoerythrin), Photosystems I and II (PSI, PSII), cytochrome b_6f, and ATP synthase (Fig. 4c, d, Supplementary Fig. 4). Since the photosystems are the primary generators of reactive oxygen species (ROS) under excessive irradiance[33,34], reducing the effective optical cross-section (via antenna reduction) and constricting electron throughput directly limit the accumulation of damaging excitation pressure[35].

MPn utilization drives a fundamental metabolic trade-off from growth to survival. Gene set enrichment analysis (GSEA) revealed a stark shift in global gene expression profiles (Fig. 4d, Supplementary Fig. 4): while phosphonate metabolism was upregulated (NES = 1.68, $q = 0.197$), pathways essential for cell growth, including ribosome biogenesis (NES = -3.70, $q < 0.001$), DNA replication (NES = -1.75, $q = 0.079$), and RNA polymerase activity (NES = -1.80, $q = 0.071$), were downregulated. Venn analysis of differentially expressed genes showed that SphR (Tery_2902), a PhoB-homologous regulator of the two-component system[36,37], was significantly upregulated across all three light levels (Fig. 4d, Supplementary Fig. 5). This PhoB regulator potentially coordinates global reprogramming by activating P-acquisition genes (including the *phn* operon) and modulating the trade-off between tolerance to high light and biomass accumulation.

Discussion

Our results substantially advance the prevailing understanding of *Trichodesmium* vertical dynamics, shifting the model from a passive, carbohydrate-ballasted process to an active, state-dependent regulatory system. We propose a conceptual framework in which nutrient stress and light availability drive populations to alternate between "Growth-Migration Mode" and "Surface-Survival Mode" (Fig. 5).

In the "Growth-Migration Mode," effective nutrient acquisition supports active growth with a diel vertical migration driven by light-regulated carbohydrate ballasting[11,12,17,18]. This cycle maintains *Trichodesmium* in an optimal subsurface niche, the lower limit of which constitutes a metabolic 'safety brake'—the buoyancy compensation depth (BCD). Defined by the minimum light threshold (> 30 µmol photons m^{-2} s^{-1}) required to generate sinking ballast (Fig. 2), the buoyancy compensation depth prevents colonies from sinking to critical depths (> 120–200 m) where hydrostatic pressure would cause irreversible gas vesicle collapse[15], thereby confining the population to subsurface waters. Accordingly, colonies observed below this physiological limit likely represent a loss of metabolic control[38], driven by passive sinking mechanisms such as senescence (Supplementary Fig. 6), mineral ballasting, or programmed cell death[6,19,38,39].

https://doi.org/10.1038/s41467-026-76233-9

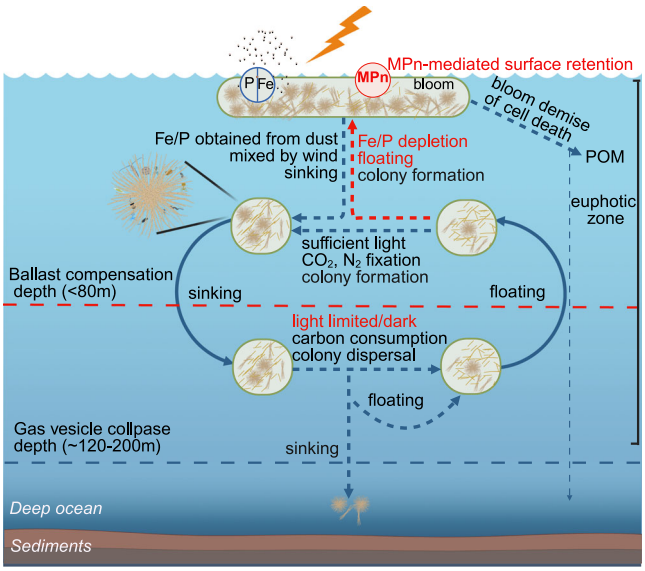


Fig. 5 | Conceptual illustration of *Trichodesmium* vertical migration and surface bloom maintenance. *Trichodesmium* generally undergoes carbohydrate-ballasted diel vertical migration (Growth-Migration Mode, blue loop). Subsurface photosynthesis accumulates carbohydrates, increasing cell density (sinking), a process often accelerated by light-induced aggregation[62]. In deeper, light-limited waters, respiratory consumption of carbohydrates restores positive buoyancy (ascent)[11,12]. Crucially, our data suggest this light-dependent consumption creates a Ballast Compensation Depth (BCD, <80 m); below this depth, net carbon fixation fails to replenish the metabolic ballast pool required for sinking, thereby triggering colonies ascent before they reach the gas vesicle collapse depth (~ 120–200 m), where hydrostatic pressure destroys gas vesicles. However, particularly dense colonies may sink directly to the deep sea[38]. Nutrient depletion overrides this cycle and leads to surface retention (red arrow): Fe/P depletion triggers floating and enhanced colony formation, facilitating access to nutrients from atmospheric dust deposition[42,44,62]. Furthermore, methylphosphonate (MPn) utilization activates a "Surface-Survival Mode", which positions gas vesicles to form a light barrier and downregulates photosynthetic activity to mitigate photodamage, thereby enabling survival under extreme surface light. Created in BioRender. Zou, C. (2026) https://BioRender.com/mwzoqxe.

While this carbohydrate model explains diel migration in subsurface waters, it fails to account for the persistence of surface blooms[5]. We address this paradox by demonstrating that nutrient starvation acts as the primary driver disrupting the migration cycle. Unlike other bloom-forming cyanobacteria such as *Anabaena circinalis* or *Microcystis aeruginosa*, which lose buoyancy during nutrient stress[40,41], *Trichodesmium* actively retains surface buoyancy under Fe or P depletion (Fig. 1). This distinctive "starvation response" likely represents a specialized evolutionary adaptation to the oligotrophic ocean, maintaining populations in the surface waters to maximize interception and utilization of surface nutrient sources such as atmospheric dust and its associated nutrients[42,43,44].

Central to this surface-retention strategy is the utilization of methylphosphonate (MPn) during periods of inorganic phosphorus limitation[29], which can especially occur during the mass accumulation of *Trichodesmium* biomass on the surface of the tropical oceans[45]. While labile phosphorus supports rapid growth and sinking phenotypes, assimilation of MPn activates a "Surface-Survival Mode", which enforces a buoyant phenotype and induces a profound structural remodeling: the relocalization of gas vesicles to the cell periphery (Figs. 2, 3). This dynamic plasticity transforms gas vesicles from simple buoyancy devices into an optical "shield" that scatters incident light, providing a mechanistic explanation for the peripheral gas vesicle distribution typically observed in surface ocean populations[17,22,32]. Crucially, this structural defense is coupled with a metabolic trade-off: a global repression of photosynthetic machinery. Given that the photosystems are the primary generator of reactive oxygen species (ROS)[33,34], reducing the antenna cross-section and constricting electron throughput directly minimizes ROS generation (Fig. 4)[35]. This metabolic trade-off coincides with a broad downregulation of growth processes, including ribosome biogenesis and DNA/RNA replication (Fig. 4). Thus, the population shifts from a growth-oriented state to a persistence-oriented state, prioritizing stress tolerance over rapid biomass accumulation to endure the hostile radiative environment of surface waters.

Based on these findings, we propose a refined model of bloom development (Fig. 5), in which *Trichodesmium*'s initial proliferation occurs in subsurface waters, whereas surface blooms represent a terminal growth stage driven by nutrient exhaustion. This mechanism reconciles field observations: in the P-limited VAHINE mesocosm experiment, surface accumulation lagged behind the initial growth phase, appearing after a distinct phosphate drawdown[6,45,46]; similarly, on the Fe-limited West Florida Shelf, while dust deposition initiates production, the persistence of surface blooms coincides with the subsequent exhaustion of phosphorus[47]. Viewing surface blooms as the visible signature of subsurface nutrient exhaustion, our framework predicts that in a warming ocean, where intensified stratification further limits nutrient supply[48–51], there may be a shift toward smaller, more ephemeral surface populations. Ultimately, by linking nutrient-driven ascent with MPn-mediated surface persistence (Fig. 5), this study provides a unified physiological basis for anticipating the resilience and distribution of *Trichodesmium* blooms in the future ocean.

Methods

Culture conditions

Stock cultures of *Trichodesmium* IMS101 were maintained in nitrogen-free YBCII medium[26], supplemented with 50 µM phosphate. The cultures were grown at 27 ± 1 °C under a light intensity of 110 µmol photons m^{-2} s^{-1}, following a 12 h:12 h light:dark cycle using white LED tubes. In Experiment I (corresponding to Fig. 1): to define the buoyancy response to specific nutrient limitations, two parallel setups were established. First, for iron limitation, *Trichodesmium* was grown in batch cultures. Filaments were collected, washed thoroughly with iron-free medium, and resuspended in YBCII medium lacking added iron but supplemented with 20 µM EDTA. Cultures were maintained at a light intensity of 150 µmol photons m^{-2} s^{-1}. For the iron-replete group, 0.4 µM $FeCl_3$ was added. Buoyancy was assessed and photographed on day 14, when the iron-depleted population accumulated at the surface following the exhaustion of intracellular iron reserves and residual background iron. Second, regarding phosphorus availability, filaments were washed with phosphorus-free medium and inoculated into batch cultures with varying phosphate concentrations (0, 0.5, 1, and 5 µM) in batch mode, with phenotypes recorded on day 15. Additionally, to ensure stable physiological states, cultures were maintained under phosphorus-replete (5 µM) and phosphorus-limited (0.5 µM) conditions in semi-continuous mode for two months prior to assessment. In Experiment II (corresponding to Figs. 1 and 3), we investigated the effects of different phosphorus sources. YBCII medium was modified to contain 5 µM of specific phosphorus compounds serving as the sole P source. These treatments included phosphate esters (glycerol-3-phosphate, fructose-1,6-bisphosphate, and adenosine-5-phosphate), phosphonate (2-aminoethylphosphonate), and polyphosphate (tripolyphosphate), representing phosphorus-replete conditions. In addition, inorganic phosphate (5 µM, Pi^+), a phosphorus-limited (0.5 µM, Pi^-) control group were included, as described in the experiment I. All cultures were maintained in an iron-replete, semi-continuous mode at a light intensity of 150 µmol photons m^{-2} s^{-1}, and diluted every 3–5 days. Following a two-month acclimation period, buoyancy was measured (see below). Subsequently, the cultures were exposed to

high irradiance (900 µmol photons m^{-2} s^{-1}) to evaluate their high-light response. In Experiment III (presenting results for Figs. 2, 3, and 4), to assess long-term light adaptation, *Trichodesmium* was grown in semi-continuous cultures across six light intensities (30, 60, 110, 220, 370, and 680 µmol photons m^{-2} s^{-1}), using either 50 µM phosphate (Pi) or methylphosphonate (MPn) as the phosphorus source. Cultures were acclimated for one year prior to physiological measurements. Notably, cultures supplied with Pi could not be sustained at the highest irradiance (680 µmol photons m^{-2} s^{-1}), despite three independent attempts to establish the culture.

Buoyancy assay

Buoyancy was quantified as the vertical migration rate using the SETCOL method[52,53]. To ensure consistent experimental conditions, the ascent and descent rates were measured in an incubator (HP300G-C, Ruihua, China). Briefly, 50 mL of subsamples were taken from the initial culture (B_1) and after 2 h (B_2) of incubation to measure the chlorophyll *a* (Chl *a*) concentration and correct for growth during the settling period. The culture suspension was mixed thoroughly, poured into a settling column and left undisturbed for 2 h. After settling, Chl *a* concentration of the upper column (B_u) region was measured. Subsequently, the culture from the middle fraction was carefully drained, and the Chl *a* concentration of the settled (bottom) fraction (B_s) was determined. The ascent rates (A) and descent rates (D) were calculated using the formula of the SETCOL method[52,53]:

$$A = \frac{V_u \times [B_u - (B_1 + B_2)/2]}{V_t \times (B_1 + B_2)/2} \times \frac{l}{t} \quad (1)$$

$$D = \frac{V_s \times [B_s - (B_1 + B_2)/2]}{V_t \times (B_1 + B_2)/2} \times \frac{l}{t} \quad (2)$$

where V_u, V_s, and V_t represent the volumes of the upper compartment, settled compartment, and total column, respectively; l is the column height (m); t is the settling duration (2 h).

Chlorophyll *a* content

For chlorophyll *a* (Chl *a*) quantification, filaments were filtered onto GF/F filters (25 mm, Whatman, USA) and extracted in absolute methanol at 4 °C for 12 h in the dark. Extracts were centrifuged at 12,000 *g* for 4 min, and the supernatants were scanned for absorbance from 250 to 800 nm using a Cary 60 spectrophotometer (Agilent, CA, USA). Chl *a* concentration was calculated using the following formula[54]:

$$Chl\,a\ \left(\mu g\ mL^{-1}\right) = \frac{12.9447 \times V_e(OD_{665} - OD_{750})}{V_s} \quad (3)$$

where OD_{665} and OD_{750} are the absorbances at wavelengths 665 nm and 750 nm respectively; V_e and V_s are the volumes of the extract and the filtered sample.

Specific growth rate

Specific growth rate (μ) was derived from the Chl *a* concentration using the equation:

$$\mu\left(d^{-1}\right) = \frac{\ln m_2 - \ln m_1}{t_2 - t_1} \quad (4)$$

where m_2 and m_1 represent the Chl *a* concentrations at times t_2 and t_1.

Chlorophyll fluorescence measurements

Rapid light curves (RLCs, Supplementary Fig. 7) were generated using Multi-color PAM (Walz, Germany) across 11 actinic light intensities [*E*] from 5 to 2904 µmol photons m^{-2} s^{-1} with 30 s exposures each. Data were fitted to the Eilers-Peeters model[55]:

$$rETR = \frac{E}{a \times E^2 + b \times E + c} \quad (5)$$

where a, b, and c are the fitting coefficients. Relative photosynthetic light-harvesting efficiency (initial slopes, α) and maximum relative electron transport rate ($rETR_{max}$) were derived as:

$$\alpha = \frac{1}{c} \quad (6)$$

$$rETR_{max} = \frac{1}{(b + 2 \times \sqrt{a \times c})} \quad (7)$$

Carbon and nitrogen assimilation

The assimilation rates for carbon and nitrogen were evaluated by monitoring changes in particulate organic carbon (POC) and particulate organic nitrogen (PON) over a 12 h period. Samples were collected at the onset of the light period and after 12 h, filtered onto pre-combusted GF/F filters (450 °C for 4 h), and rinsed with 100 mL of nitrogen-free YBCII. The filters were acidified with HCl fumes for 24 h, and dried at 60 °C for another 24 h to remove unassimilated inorganic carbon. POC and PON were quantified using an elemental analyzer (vario EL cube, Elementar, Germany).

Phosphorus assimilation

Phosphorus assimilation rates were determined by measuring particulate phosphorus (PP) accumulation over a 12 h light period following the Solórzano method[56]. Samples were filtered onto pre-combusted GF/F filters and rinsed with 100 mL of phosphorus-free YBCII. Filters were then soaked in 0.017 M $MgSO_4$, dried at 95 °C, and baked at 450 °C for 2 h. Prior to analysis, samples were hydrolyzed with 0.2 M HCl at 80 °C for 30 min, and analyzed using an auto-analyzer (AA3, Seal, Germany).

Gas vesicle content

Relative gas vesicle content was quantified as the percentage of vesicle area relative to the total cell area in transmission electron micrographs, analyzed using ImageJ. At least 25 cells were analyzed for each condition. For sample preparation, filaments were fixed in 2% (v/v) glutaraldehyde in seawater at 27 °C for 1 h, then kept at 4 °C overnight. After centrifugation at 500 *g*, the filaments were embedded in 2% low-melting-point agar and post-fixed in 2% glutaraldehyde at 4 °C overnight. Samples were rinsed three times with phosphate buffer (PB) for 15 min each, then stained with 2% (w/v) osmium tetroxide (OsO_4) in PB at 4 °C for 2 h, and rinsed again three times. Desalting was performed using a graded series of PB dilutions in distilled water (75%, 50%, 25%, and 0%) for 15 min at room temperature. Dehydration was achieved using 30% and 50% ethanol for 15 min each, followed by overnight staining with 2% uranyl acetate in 70% ethanol. After three rinses, samples were further dehydrated in 90% and 100% ethanol for 15 min each. The samples were then dehydrated by a series of acetone dilutions (25%, 50%, 75%, and 100% in ethanol) for 15 min each. Filaments were infiltrated sequentially with Epon 812 resin in acetone at concentrations of 25% (45 min), 50% (2 h), 75% (2 h), and 100% (overnight). Excess resin was removed, and samples were kept at 70 °C for 24 h. After cooling, the embedded cells were sectioned into 75 nm slices and imaged using an electron microscope (Hitachi HT-7800, Japan). Transmission electron microscopy (TEM) images were obtained of longitudinal sections at 3000x magnification and cross-sections at 4000x magnification.

Gas vesicle arrangement

To examine the arrangement of gas vesicles, fresh filaments were collected and imaged at 400× magnification using a light microscope (Nikon ECLIPSE Ts-FL, Japan). Gas vesicle arrangement patterns were classified into three categories: random, half-surrounding, and surrounding the cell periphery. For each treatment, we analyzed at least 300 cells to ensure robust estimates.

RNA extraction

Trichodesmium IMS101 was maintained in semi-continuous cultures supplemented with either 50 µM methylphosphonate or phosphate under three light intensities (30, 60, and 370 µmol photons m^{-2} s^{-1}). Each treatment included three biological replicates. Samples were filtered onto polycarbonate filters (5 µm, Whatman, UK) at the mid-light cycle, immediately frozen in liquid nitrogen, and stored at -80 °C. Total RNA was extracted using TRIzol Reagent (Life Technologies, CA, USA). RNA quality and integrity were assessed by agarose gel electrophoresis and a Bioanalyzer 2100 (Agilent, CA, USA), and concentrations were measured with a NanoPhotometer® spectrophotometer (Implen, CA, USA).

Transcriptome sequencing and analysis

Total RNA (1 µg) was used for cDNA library construction. Ribosomal RNA (rRNA) was depleted using the Illumina Ribo-Zero rRNA Removal Kit (Illumina, USA). cDNA libraries were prepared with the NEBNext Ultra II RNA Library Prep Kit (New England Biolabs, USA) and purified with Agencourt AMPure XP beads (Beckman Coulter,USA). Library amplification and clustering were performed using NEBNext Q5 Hot Start HiFi PCR Master Mix (New England Biolabs, USA) on a cBot Cluster Generation System. Sequencing was conducted on the Illumina Novaseq 6000 platform, generating 150 bp paired-end reads. Raw data were processed using fastp (version 0.18.0)[57] to trim adapters from reads and to remove those with over 10% unknown nucleotides, and low-quality reads (where > 50% of bases had a Phred quality score $Q \leq 20$). Clean reads were mapped to the *Trichodesmium* IMS101 genome (Genome ID 2606217490), obtained from the Integrated Microbial Genomes (IMG) database (https://img.jgi.doe.gov/), using Bowtie 2 (version 2.2.8)[58]. Reads mapping to rRNA or with excessive mismatches were discarded. Gene expression levels were quantified using RSEM[59]. Differential expression analysis was performed with DESeq2 (v1.4.5)[60], using thresholds of $\log_2$ Fold Change ≥ 1 and adjusted p-value ≤ 0.05. Gene Ontology (GO) and KEGG pathway analyses were conducted using Omicsmart platform (http://www.omicsmart.com). Statistical correlations, Venn diagrams, and Principal Component Analysis (PCA) were performed in R (version 1.8.4) using the psych, VennDiagram, and gmodels packages, respectively. Gene set enrichment analysis (GSEA) was carried out using the GSEA software with the MSigDB database to identify significantly enriched GO terms and KEGG pathways[61]. Genes were ranked based on the signal-to-noise ratio of their expression levels. The enrichment score (ES) and p-values were calculated under default parameter settings.

Statistical analysis

Data are presented as mean ± sd ($n = 3$ independent biological replicates). Data normality and variance homogeneity were verified using the Shapiro–Wilk and Brown-Forsythe tests, respectively. Statistical comparisons were performed using two-sided Student's t-tests or one-way or two-way ANOVA followed by two-sided Tukey's post hoc test, and linear regression was used for correlation analyses. All tests were two-sided with $P < 0.05$ considered statistically significant.

Reporting summary

Further information on research design is available in the Nature Portfolio Reporting Summary linked to this article.

Data availability

The RNA-sequencing data generated in this study have been deposited in the Genome Sequence Archive (GSA) database under accession code CRA038782. Source data are provided with this paper.

References

1. Capone, D. G. et al. *Trichodesmium*, a globally significant marine cyanobacterium. *Science* **276**, 1221–1229 (1997).
2. Boatman, T. G., Upton, G. J., Lawson, T. & Geider, R. J. Projected expansion of *Trichodesmium*'s geographical distribution and increase in growth potential in response to climate change. *Glob. Chang. Biol.* **26**, 6445–6456 (2020).
3. Westberry, T. K. & Siegel, D. A. Spatial and temporal distribution of *Trichodesmium* blooms in the world's oceans. *Glob. Biogeochem. Cycles* **20**. https://doi.org/10.1029/2005GB002673 (2006)
4. Lu, Y. et al. Effect of light on N_2 fixation and net nitrogen release of *Trichodesmium* in a field study. *Biogeosciences* **15**, 1–12 (2018).
5. Sabeur, H. I., Wafa, F.-S., Asma, H. & Malika, B. H. Long term characterization of *Trichodesmium erythraeum* blooms in Gabès Gulf (Tunisia). *Cont. Shelf Res.* **124**, 95–103 (2016).
6. Spungin, D. et al. Mechanisms of *Trichodesmium* demise within the New Caledonian lagoon during the VAHINE mesocosm experiment. *Biogeosciences* **13**, 4187–4203 (2016).
7. Caffin, M. et al. Transfer of diazotroph-derived nitrogen to the planktonic food web across gradients of N_2 fixation activity and diversity in the western tropical South Pacific Ocean. *Biogeosciences* **15**, 3795–3810 (2018).
8. Zehr, J. P. & Capone, D. G. Changing perspectives in marine nitrogen fixation. *Science* **368**, eaay9514 (2020).
9. Buchanan, P. J., Chase, Z., Matear, R. J., Phipps, S. J. & Bindoff, N. L. Marine nitrogen fixers mediate a low latitude pathway for atmospheric CO_2 drawdown. *Nat. Commun.* **10**, 4611 (2019).
10. Eichner, M., Inomura, K., Pierella Karlusich, J. J. & Shaked, Y. Better together? Lessons on sociality from *Trichodesmium*. *Trends Microbiol* **31**, 1072–1084 (2023).
11. Villareal, T. A. & Carpenter, E. J. Diel buoyancy regulation in the marine diazotrophic cyanobacterium *Trichodesmium thiebautii*. *Limnol. Oceanogr.* **35**, 1832–1837 (1990).
12. Villareal, T. A. & Carpenter, E. J. Buoyancy regulation and the potential for vertical migration in the oceanic cyanobacterium *Trichodesmium*. *Microb. Ecol.* **45**, 1–10 (2003).
13. White, A. E., Spitz, Y. H. & Letelier, R. M. Modeling carbohydrate ballasting by *Trichodesmium* spp. *Mar. Ecol. Prog. Ser.* **323**, 35–45 (2006).
14. Romans, K. M., Carpenter, E. J. & Bergman, B. Buoyancy regulation in the colonial diazotrophic cyanobacterium *Trichodesmium tenue*: ultrastructure and storage of carbohydrate, polyphosphate, and nitrogen. *J. Phycol.* **30**, 935–942 (1994).
15. Walsby, A. E. The properties and buoyancy-providing role of gas vacuoles in *Trichodesmium* Ehrenberg. *Br. Phycol. J.* **13**, 103–116 (1978).
16. Huber, S. T., Terwiel, D., Evers, W. H., Maresca, D. & Jakobi, A. J. Cryo-EM structure of gas vesicles for buoyancy-controlled motility. *Cell* **186**, 975–986 (2023).
17. Walsby, A. E. Gas vesicles. *Microbiol. Rev.* **58**, 94–144 (1994).
18. Held, N. A. et al. Dynamic diel proteome and daytime nitrogenase activity supports buoyancy in the cyanobacterium *Trichodesmium*. *Nat. Microbiol.* **7**, 300–311 (2022).
19. Berman-Frank, I., Bidle, K. D., Haramaty, L. & Falkowski, P. G. The demise of the marine cyanobacterium, *Trichodesmium* spp., via an autocatalyzed cell death pathway. *Limnol. Oceanogr.* **49**, 997–1005 (2004).
20. Cai, X. et al. Electron transport kinetics in the diazotrophic cyanobacterium *Trichodesmium* spp. grown across a range of light levels. *Photosynth. Res.* **124**, 45–56 (2015).

21. Carpenter, E. J. & Price, C. C. Marine *Oscillatoria* (*Trichodesmium*): Explanation for aerobic nitrogen fixation without heterocysts. *Science* **191**, 1278–1280 (1976).
22. Van Baalen, C. & Brown, R. M. The ultrastructure of the marine blue green alga, *Trichodesmium erythraeum*, with special reference to the cell wall, gas vacuoles, and cylindrical bodies. *Arch. Mikrobiol.* **69**, 79–91 (1969).
23. Kelman, D., Ben-Amotz, A. & Berman-Frank, I. Carotenoids provide the major antioxidant defence in the globally significant N_2-fixing marine cyanobacterium *Trichodesmium*. *Environ. Microbiol.* **11**, 1897–1908 (2009).
24. Chen, C.-C. et al. Nickel superoxide dismutase protects nitrogen fixation in *Trichodesmium*. *Limnol. Oceanogr. Lett.* **7**, 363–371 (2022).
25. Chen, H.-Y. S., Niedzwiedzki, D. M., Bandyopadhyay, A., Biswas, S. & Pakrasi, H. B. A novel mode of photoprotection mediated by a cysteine residue in the chlorophyll protein IsiA. *mBio* **12**, e03663–20 (2021).
26. Chen, Y. B., Zehr, J. P. & Mellon, M. Growth and nitrogen fixation of the diazotrophic filamentous nonheterocystous cyanobacterium *Trichodesmium* sp. IMS 101 in defined media: evidence for a circadian rhythm. *J. Phycol.* **32**, 916–923 (1996).
27. Repeta, D. J. et al. Marine methane paradox explained by bacterial degradation of dissolved organic matter. *Nat. Geosci.* **9**, 884–887 (2016).
28. Sosa, O. A. et al. Phosphonate cycling supports methane and ethylene supersaturation in the phosphate-depleted western North Atlantic Ocean. *Limnol. Oceanogr.* **65**, 2443–2459 (2020).
29. Dyhrman, S. T. et al. Phosphonate utilization by the globally important marine diazotroph *Trichodesmium*. *Nature* **439**, 68–71 (2006).
30. Piazena, H., Perez-Rodrigues, E., Häder, D.-P. & Lopez-Figueroa, F. Penetration of solar radiation into the water column of the central subtropical Atlantic Ocean—optical properties and possible biological consequences. *Deep Sea Res. Part II Top. Stud. Oceanogr.* **49**, 3513–3528 (2002).
31. Bar-Zeev, E., Avishay, I., Bidle, K. D. & Berman-Frank, I. Programmed cell death in the marine cyanobacterium *Trichodesmium* mediates carbon and nitrogen export. *ISME J* **7**, 2340–2348 (2013).
32. Andresen, E. et al. Acclimation of *Trichodesmium erythraeum* ISM101 to high and low irradiance analysed on the physiological, biophysical and biochemical level. *New Phytol* **185**, 173–188 (2010).
33. Latifi, A., Ruiz, M. & Zhang, C.-C. Oxidative stress in cyanobacteria. *FEMS Microbiol. Rev.* **33**, 258–278 (2009).
34. Murata, N., Takahashi, S., Nishiyama, Y. & Allakhverdiev, S. I. Photoinhibition of photosystem II under environmental stress. *Biochim. Biophys. Acta Bioenerg.* **1767**, 414–421 (2007).
35. Huner, N. P. A., Öquist, G. & Sarhan, F. Energy balance and acclimation to light and cold. *Trends Plant Sci* **3**, 224–230 (1998).
36. Suzuki, S., Ferjani, A., Suzuki, I. & Murata, N. The SphS-SphR two component system is the exclusive sensor for the induction of gene expression in response to phosphate limitation in *Synechocystis*. *J. Biol. Chem.* **279**, 13234–13240 (2004).
37. Frischkorn, K. R., Haley, S. T. & Dyhrman, S. T. Transcriptional and proteomic choreography under phosphorus deficiency and resupply in the N_2 fixing cyanobacterium *Trichodesmium erythraeum*. *Front. Microbiol.* **10**, 330 (2019).
38. Benavides, M. et al. Sinking *Trichodesmium* fixes nitrogen in the dark ocean. *ISME J* **16**, 2398–2405 (2022).
39. Wang, S. et al. Costs of dust collection by *Trichodesmium*: effect on buoyancy and toxic metal release. *J. Geophys. Res. Biogeosci.* **129**, e2023JG007954 (2024).
40. Konopka, A., Kromkamp, J. C. & Mur, L. R. Buoyancy regulation in phosphate-limited cultures of *Microcystis aeruginosa*. *FEMS Microbiol. Ecol.* **3**, 135–142 (1987).
41. Brookes, J. D., Ganf, G. G., Green, D. & Whittington, J. The influence of light and nutrients on buoyancy, filament aggregation and flotation of *Anabaena circinalis*. *J. Plankton Res.* **21**, 327–341 (1999).
42. Rubin, M., Berman-Frank, I. & Shaked, Y. Dust- and mineral-iron utilization by the marine dinitrogen-fixer *Trichodesmium*. *Nat. Geosci.* **4**, 529–534 (2011).
43. Shaked, Y. et al. Co-acquisition of mineral-bound iron and phosphorus by natural *Trichodesmium* colonies. *Limnol. Oceanogr.* **68**, 1064–1077 (2023).
44. Tzubari, Y., Magnezi, L., Be'er, A. & Berman-Frank, I. Iron and phosphorus deprivation induce sociality in the marine bloom-forming cyanobacterium *Trichodesmium*. *ISME J* **12**, 1682–1693 (2018).
45. Gimenez, A., Baklouti, M., Bonnet, S. & Moutin, T. Biogeochemical fluxes and fate of diazotroph-derived nitrogen in the food web after a phosphate enrichment: modeling of the VAHINE mesocosms experiment. *Biogeosciences* **13**, 5103–5120 (2016).
46. Bonnet, S. et al. Introduction to the project VAHINE: VAriability of vertical and tropHIc transfer of diazotroph derived N in the south wEst Pacific. *Biogeosciences* **13**, 2803–2814 (2016).
47. Lenes, J. M. et al. Iron fertilization and the *Trichodesmium* response on the West Florida shelf. *Limnol. Oceanogr.* **46**, 1261–1277 (2001).
48. Stocker, T. Climate change 2013: the physical science basis: Working Group I contribution to the Fifth assessment report of the Intergovernmental Panel on Climate Change. (Cambridge University Press, 2014).
49. Cheng, L. et al. New Record Ocean Temperatures and Related Climate Indicators in 2023. *Adv. Atmos. Sci.* https://doi.org/10.1007/s00376-024-3378-5 (2024).
50. Kwiatkowski, L. et al. Twenty-first century ocean warming, acidification, deoxygenation, and upper-ocean nutrient and primary production decline from CMIP6 model projections. *Biogeosciences* **17**, 3439–3470 (2020).
51. Li, G. et al. Increasing ocean stratification over the past half-century. *Nat. Clim. Chang.* **10**, 1116–1123 (2020).
52. Bienfang, P. K. SETCOL — A Technologically Simple and Reliable Method for Measuring Phytoplankton Sinking Rates. *Can. J. Fish. Aquat. Sci.* **38**, 1289–1294 (1981).
53. Cavan, E. L., Trimmer, M., Shelley, F. & Sanders, R. Remineralization of particulate organic carbon in an ocean oxygen minimum zone. *Nat. Commun.* **8**, 14847 (2017).
54. Ritchie, R. J. Consistent sets of spectrophotometric chlorophyll equations for acetone, methanol and ethanol solvents. *Photosynth. Res.* **89**, 27–41 (2006).
55. Eilers, P. & Peeters, J. A model for the relationship between light intensity and the rate of photosynthesis in phytoplankton. *Ecol. Modell.* **42**, 199–215 (1988).
56. Solórzano, L. & Sharp, J. H. Determination of total dissolved phosphorus and particulate phosphorus in natural waters. *Limnol. Oceanogr.* **25**, 754–758 (1980).
57. Chen, S., Zhou, Y., Chen, Y. & Gu, J. fastp: an ultra-fast all-in-one FASTQ preprocessor. *Bioinformatics* **34**, i884–i890 (2018).
58. Langmead, B. & Salzberg, S. L. Fast gapped-read alignment with Bowtie 2. *Nat. Methods* **9**, 357–359 (2012).
59. Li, B. & Dewey, C. N. RSEM: accurate transcript quantification from RNA-Seq data with or without a reference genome. *BMC Bioinformatics* **12**, 323 (2011).
60. Love, M. I., Huber, W. & Anders, S. Moderated estimation of fold change and dispersion for RNA-seq data with DESeq2. *Genome Biol.* **15**, 1–21 (2014).

61. Subramanian, A. et al. Gene set enrichment analysis: A knowledge-based approach for interpreting genome-wide expression profiles. *Proc. Natl. Acad. Sci. USA* **102**, 15545–15550 (2005).
62. Pfreundt, U. et al. Controlled motility in the cyanobacterium *Trichodesmium* regulates aggregate architecture. *Science* **380**, 830–835 (2023).

Acknowledgements

We are grateful to the laboratory engineers Xianglan Zeng and Wenyan Zhao for their technical and logistical supports. We also thank Caiming Wu, Luming Yao and Wei Han from the Core Facility of Biomedical Sciences, School of Life Sciences, Xiamen University for assistance with electron microscopy. Gemini was utilized to assist with language editing and proofreading.

Author contributions

K.G. and C.Z. conceived and designed the experiments. C.Z. performed the experiments and analyses. C.Z., G.G., X.L., I.B.-F., M.B. and K.G. analyzed the data and contributed to the writing and editing of the manuscript.

Funding

The work was supported by the National Natural Science Foundation of China (grant nos. 42506094 to C.Z. and 42361144840 and 41720104005 to K.G.), and the joint NSFC-Israel Science Foundation (ISF) grant (no. 3051/23) to I.B-F.

Competing interests

The authors declare no competing interests.

Additional information

Supplementary information The online version contains supplementary material available at https://doi.org/10.1038/s41467-026-76233-9.

Correspondence and requests for materials should be addressed to Kunshan Gao.

Peer review information *Nature Communications* thanks Douglas Risser and the other anonymous reviewer(s) for their contribution to the peer review of this work. A peer review file is available.

Reprints and permissions information is available at http://www.nature.com/reprints

Publisher's note Springer Nature remains neutral with regard to jurisdictional claims in published maps and institutional affiliations.

Open Access This article is licensed under a Creative Commons Attribution-NonCommercial-NoDerivatives 4.0 International License, which permits any non-commercial use, sharing, distribution and reproduction in any medium or format, as long as you give appropriate credit to the original author(s) and the source, provide a link to the Creative Commons licence, and indicate if you modified the licensed material. You do not have permission under this licence to share adapted material derived from this article or parts of it. The images or other third party material in this article are included in the article's Creative Commons licence, unless indicated otherwise in a credit line to the material. If material is not included in the article's Creative Commons licence and your intended use is not permitted by statutory regulation or exceeds the permitted use, you will need to obtain permission directly from the copyright holder. To view a copy of this licence, visit http://creativecommons.org/licenses/by-nc-nd/4.0/.

© The Author(s) 2026